Chapter 4
Results and discussion

Doping effect on physical, electrical, and optical properties of PLZT (3/52/48) ceramics is shown and discussed in this chapter.

4.1 Characterization of PLZT powder

4.1.1 Determination of calcining temperature for PLZT powder

The calcining temperature of PLZT powder was determined by performing heat treatment of the samples at different temperatures and detecting a perovskite phase. Fig. 4.1 shows the X-ray diffraction patterns of raw PLZT powder calcined at 850, 900 and 950 °C for 10 h and of PLZT sample sintered at 1250 °C for 2 h. Calcined powder at 850 °C showed a mixture of $PbZrO_3$ and $PbTiO_3$ while a single-phase perovskite with partial crystallization was observed in PLZT calcined at 900 °C. A single peak of the plane (111) and two peaks of planes (002) and (200) indicated the crystallization of tetragonal perovskite phases. [3,52,53] They were observed in the powder calcined at 950 °C for 10 h. Hence this temperature was selected for the calcining condition of PLZT powder which was similar to the condition of Poosanaas in 1999.[3] In addition, PLZT sample sintered at 1250 °C for 2 h shows the single phase of tetragonal perovskite with high crystallinity as shown in the same figure.

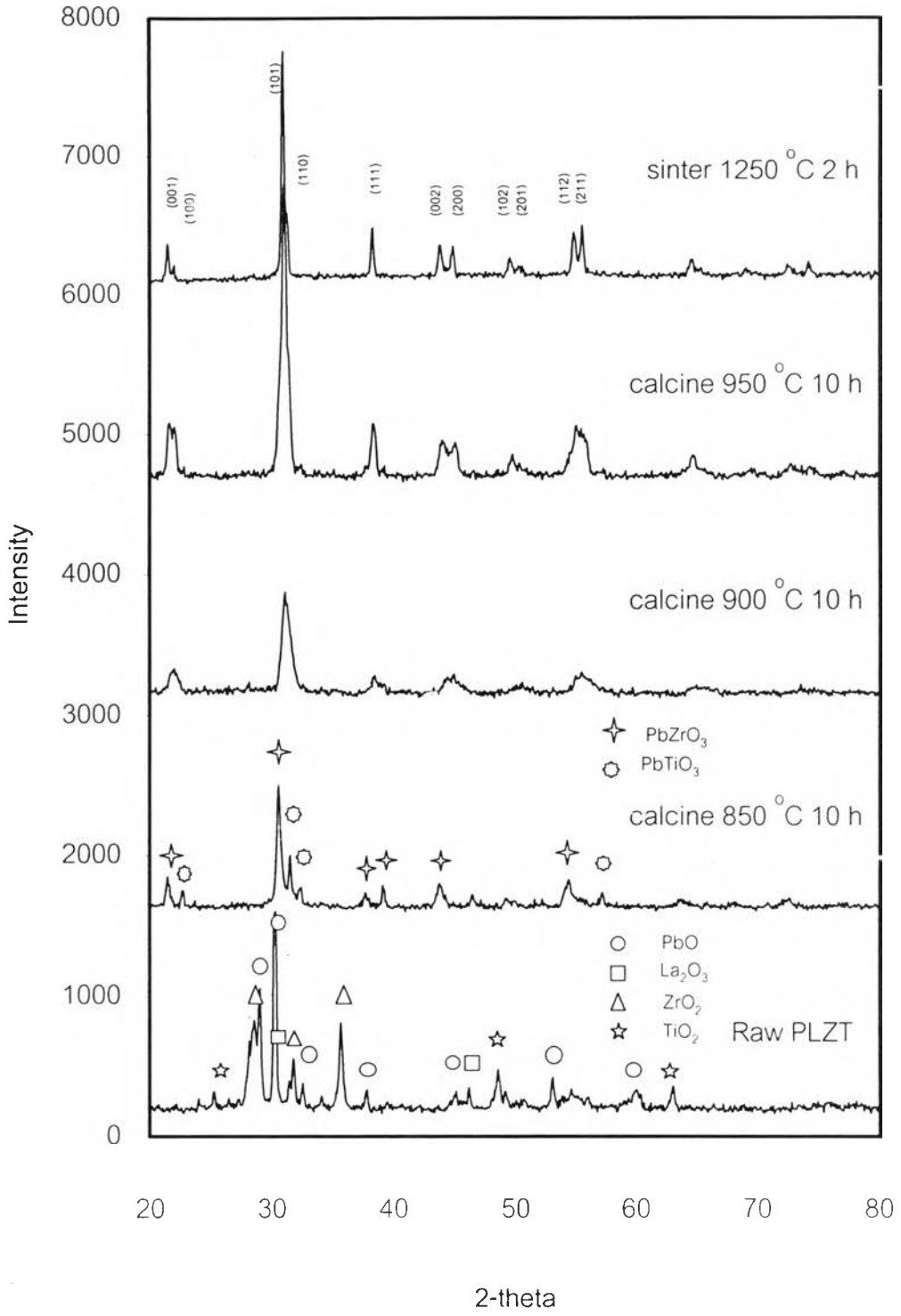

Fig. 4.1 XRD patterns of PLZT (3/52/48) powder under different heat treatment and sintered sample

4.1.2 Microstructure of calcined PLZT powder

SEM micrographs of calcined powder prepared by a conventional oxide mixing method are shown in Fig. 4.2 and 4.3. Fig. 4.2 shows as-calcined powder before milling of which agglomerated particles was clearly observed. Fig. 4.3 shows the dispersion of powder after milling for 10 h. Average particle size of milled powder is in the range of 0.6 – 0.8 μm.

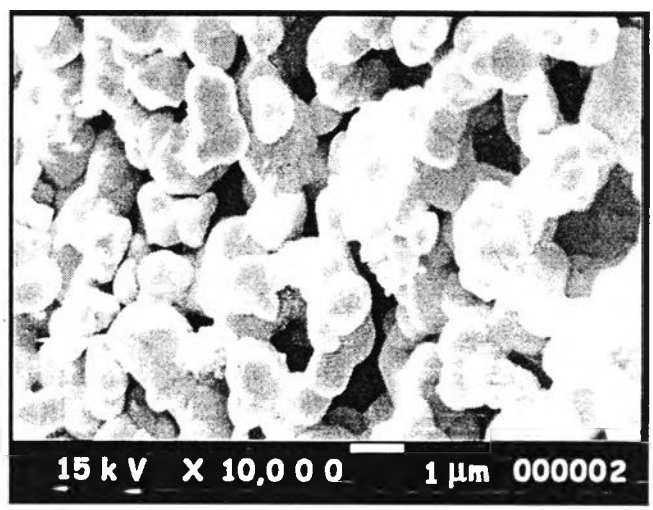

Fig. 4.2 SEM micrograph of PLZT (3/52/48) powder calcined at 950 °C for 10 h (before milling)

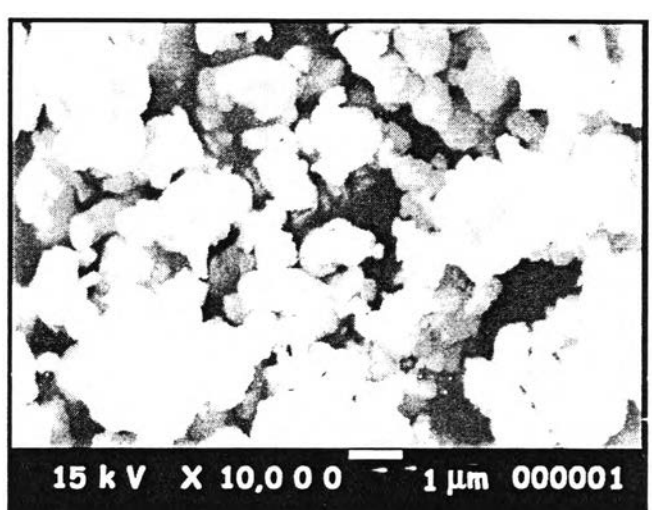

Fig. 4.3 SEM micrograph of calcined PLZT (3/52/48) powder after milling for 10 h

4.2 Dependence of lattice parameters on dopants

Lattice parameters of all doped PLZT samples were determined by the values of d-spacing of (002) and (200) peaks. Table 4.1 shows the variation of lattice parameters with the types of dopant. Theoretical density or X-ray density is calculated from the predicted molecular weight which according to the formulas in Table 2.2 or 2.3.

Table 4.1 Lattice parameters and X-ray densities of 0.5 at% doped PLZT (3/52/48) ceramics sintered at 1250 °C for 2 h

Doping Ions	Lattice parameter (Å)		tetragonality (c/a ratio)	cell volume (Å ^{3})	Molecular weight (g/mol)	X-ray density (g/cm^3)
	c	a				
Undoped	4.1339	4.0359	1.0243	67.3350	323.05	7.966
B^{3+}	4.1339	4.0496	1.0208	67.7929	322.84	7.907
Ba^{2+}	4.1301	4.0460	1.0208	67.6102	322.70	7.925
Bi^{3+}	4.1339	4.0393	1.0234	67.4485	322.97	7.951
Co^{2+}	4.1339	4.0393	1.0234	67.4485	323.17	7.956
Cr^{3+}	4.1303	4.0325	1.0243	67.1630	323.05	7.987
Cu^{2+}	4.1375	4.0393	1.0243	67.5072	323.19	7.949
Fe^{3+}	4.1375	4.0461	1.0226	67.7347	323.06	7.919
Gd^{3+}	4.1303	4.0427	1.0217	67.5032	322.71	7.938
K^{+}	4.1375	4.0393	1.0243	67.5072	322.30	7.927
Li^{+}	4.1375	4.0427	1.0234	67.6209	323.00	7.931
Mn^{3+}	4.1267	4.0359	1.0225	67.2177	323.06	7.980
Nb^{5+}	4.1339	4.0703	1.0156	68.4877	323.07	7.833
Ni^{2+}	4.1303	4.0461	1.0208	67.6168	323.17	7.936
Se^{4+}	4.1375	4.0461	1.0226	67.7347	323.09	7.920
Sn^{4+}	4.1303	4.0461	1.0208	67.6168	323.29	7.939
Sr^{2+}	4.1339	4.0427	1.0226	67.5621	322.45	7.925
V^{5+}	4.1339	4.0427	1.0226	67.5621	322.86	7.935
W^{6+}	4.1125	4.0668	1.0112	68.0161	323.44	7.896
Y^{3+}	4.1303	4.0427	1.0217	67.5032	322.37	7.930
Zn^{2+}	4.1375	4.0427	1.0234	67.6209	323.20	7.936

The tetragonality of all the samples was calculated by a "c/a" ratio. It can be seen that all the dopants reduce the tetragonality of PLZT crystal but not to a significant extend. However, Nb^{5+} and W^{6+} dopants seem to decrease the tetragonality of PLZT ceramics more than the

others. This finding is similar to the results of previous investigators.[3.52] There is no significant difference in X-ray densities of all samples. The c/a ratios are in the range of 1.0112 for W^{6+} doped and 1.0243 for undoped samples. X-ray densities are in the range of 7.832 g/cc for Nb^{5+} and 7.992 g/cc for Cr^{3+} doped samples.

Tetragonality of the samples influence the electrical properties of PLZT ceramics. It has also been found by the previous study that grain size affected the tetragonality of PZT (52/48) ceramics.[16]

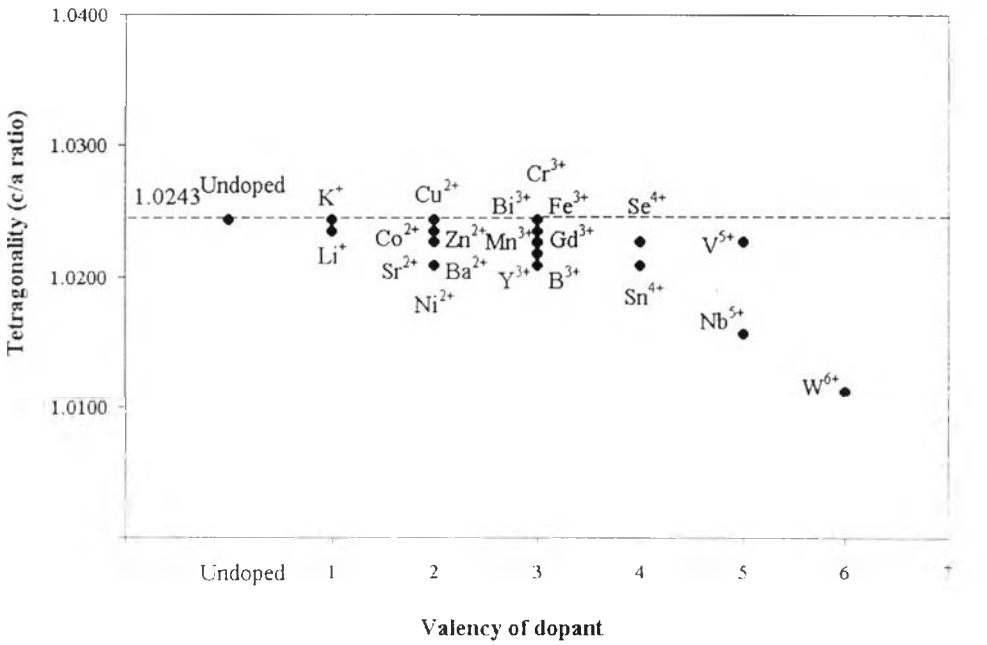

Fig. 4.4 Dopant valency as a function of tetragonality of 0.5 at% doped PLZT (3/52/48)

4.3 Density of doped PLZT ceramics

Bulk densities of the samples measured by the Archimedes method are shown in Table 4.2. The relative density is the percentage of bulk density to theoretical density. The relative densities of all the samples are in the range of 95.43 % for Ni^{2+} and 99.96 % for Nb^{5+} doped.

Table 4.2 Bulk and relative density of 0.5 at% doped PLZT (3/52/48) ceramics

Doping Ions	bulk density (g/cm^3)	theoretical density (g/cm^3)	relative density (%)
Undoped	7.827	7.966	98.26
B^{3+}	7.898	7.907	99.89
Ba^{2+}	7.819	7.925	98.66
Bi^{3+}	7.812	7.951	98.25
Co^{2+}	7.807	7.956	98.13
Cr^{3+}	7.718	7.987	96.63
Cu^{2+}	7.728	7.949	97.22
Fe^{3+}	7.858	7.919	99.23
Gd^{3+}	7.802	7.938	98.29
K^{+}	7.616	7.927	96.08
Li^{+}	7.689	7.931	96.95
Mn^{3+}	7.663	7.980	96.03
Nb^{5+}	7.829	7.833	99.95
Ni^{2+}	7.573	7.936	95.43
Se^{4+}	7.818	7.92	98.71
Sn^{4+}	7.732	7.939	97.39
Sr^{2+}	7.815	7.925	98.61
V^{5+}	7.764	7.935	97.84
W^{6+}	7.662	7.896	97.04
Y^{3+}	7.739	7.93	97.59
Zn^{2+}	7.796	7.956	98.24

4.4 Microstructure of doped PLZT ceramics

Microstructures of PLZT ceramics sintered at 1250 °C for 2 h were examined by a Scanning Electron Microscope (SEM). Fig. 4.5 a–u show the SEM micrographs of all polished and thermally etched samples. Small amounts of intergranular and intragranular pores were observed in all the samples. Okazaki, K.; Nagata, K.[6] and Yin, Z. W.[54] suggested that size and amount of porosity affected the desired properties of PLZT ceramics.

The average grain sizes were calculated from the SEM micrographs by the line intercept method. Table 4.3 shows the average grain sizes of 0.5 at% doped PLZT (3/52/48) ceramics sintered at 1250 °C for 2 h. These average grain sizes are in the range of 0.9 – 2.0 μm.

Table 4.3 Average grain size of 0.5 at% doped PLZT (3/52/48) ceramics sintered at 1250 °C for 2 h

Doping Ions	average grain size (μm)
Undoped	1.13
B^{3+}	0.90
Ba^{2+}	0.98
Bi^{3+}	1.07
Co^{2+}	1.63
Cr^{3+}	1.25
Cu^{2+}	1.12
Fe^{3+}	1.21
Gd^{3+}	1.10
K^{+}	1.34
Li^{+}	0.96

Doping Ions	average grain size (μm)
Mn^{3+}	1.34
Nb^{5+}	1.27
Ni^{2+}	1.35
Sc^{4+}	1.05
Sn^{4+}	1.20
Sr^{2+}	1.10
V^{5+}	1.12
W^{6+}	1.96
Y^{3+}	1.32
Zn^{2+}	1.50

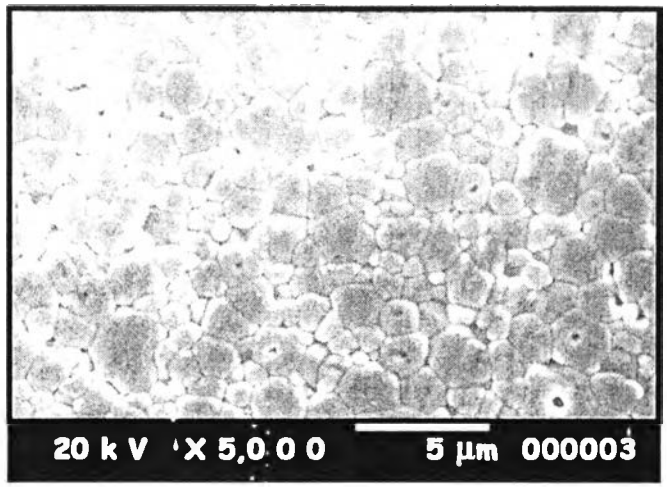

Fig. 4.5 a. SEM micrograph of undoped PLZT (3/52/48) ceramics

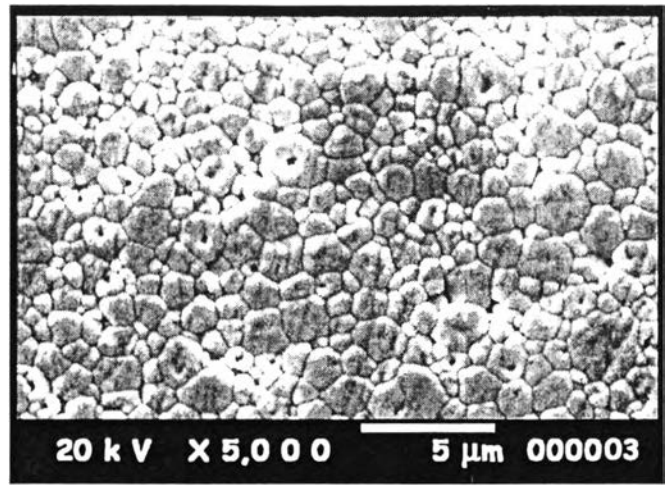

Fig. 4.5 b. SEM micrograph of 0.5 at% B_2O_3 doped PLZT (3/52/48) ceramics

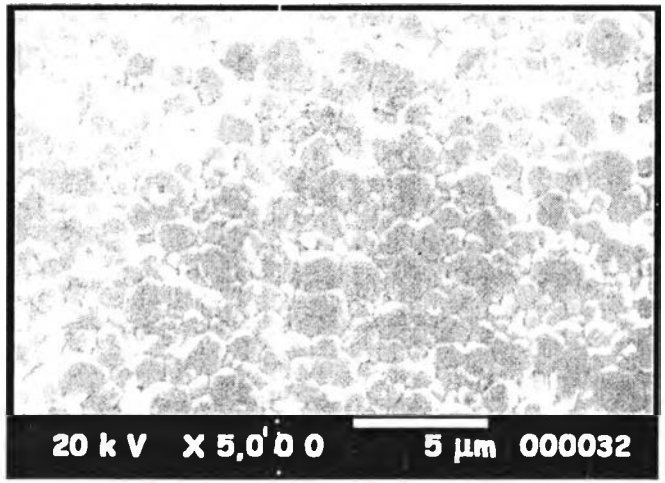

Fig. 4.5 c. SEM micrograph of 0.5 at% BaO doped PLZT (3/52/48) ceramics

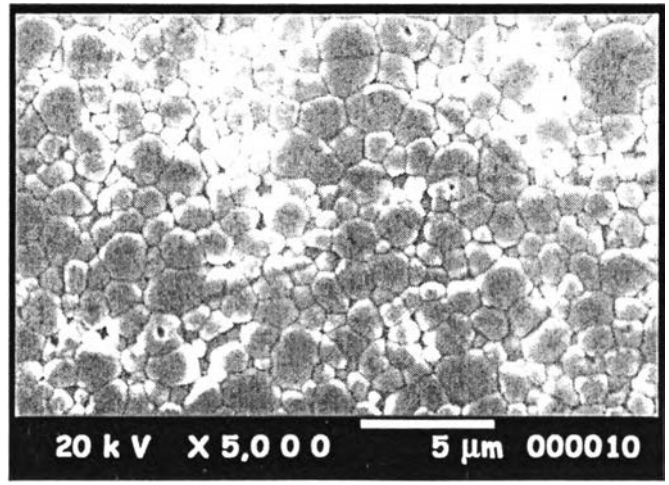

Fig. 4.5 d. SEM micrograph of 0.5 at% Bi_2O_3 doped PLZT (3/52/48) ceramics

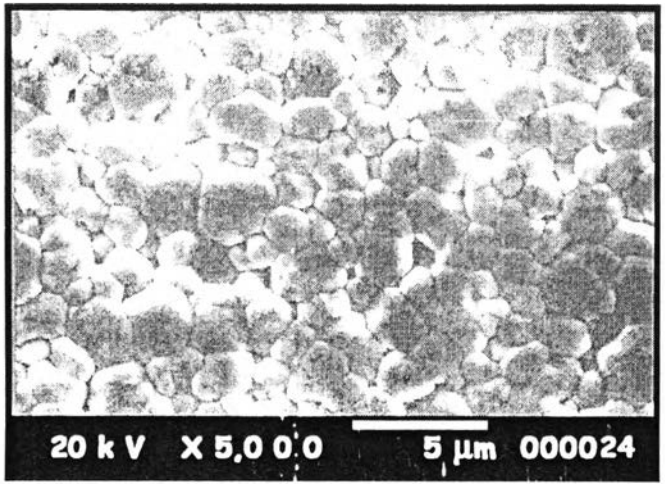

Fig. 4.5 e. SEM micrograph of 0.5 at% CoO doped PLZT (3/52/48) ceramics

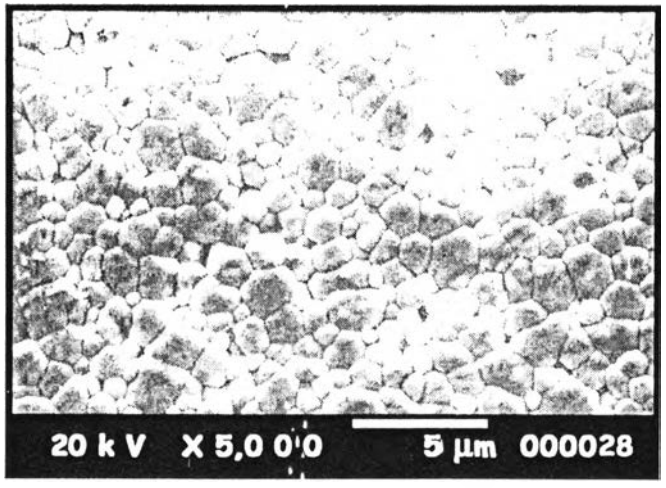

Fig. 4.5 g. SEM micrograph of 0.5 at% CuO doped PLZT (3/52/48) ceramics

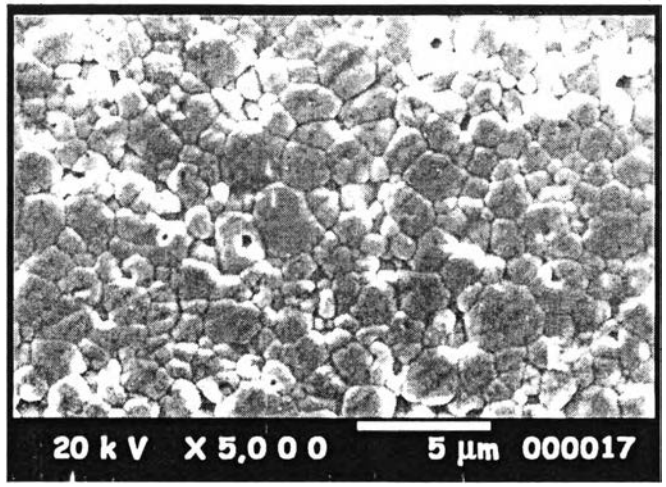

Fig. 4.5 f. SEM micrograph of 0.5 at% Cr_2O_3 doped PLZT (3/52/48) ceramics

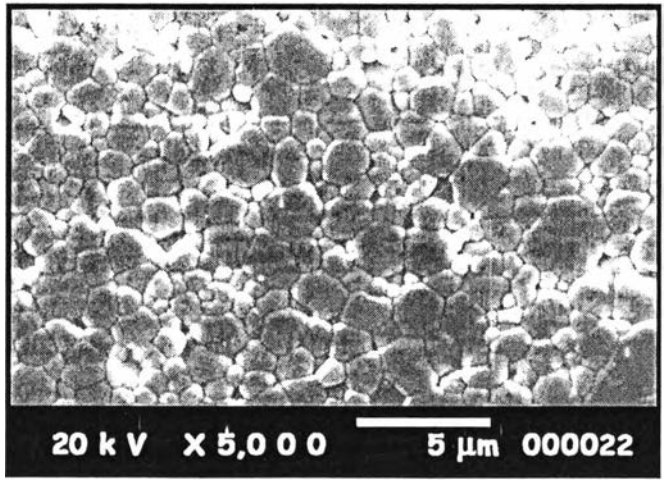

Fig. 4.5 h. SEM micrograph of 0.5 at% Fe_2O_3 doped PLZT (3/52/48) ceramics

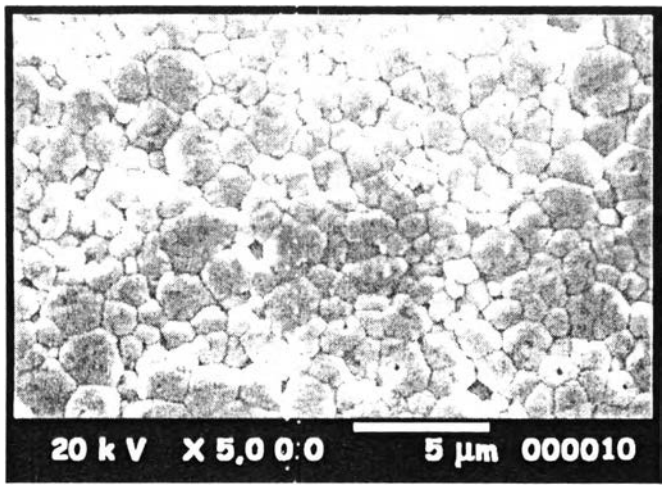

Fig. 4.5 i. SEM micrograph of 0.5 at% Gd_2O_3 doped PLZT (3/52/48) ceramics

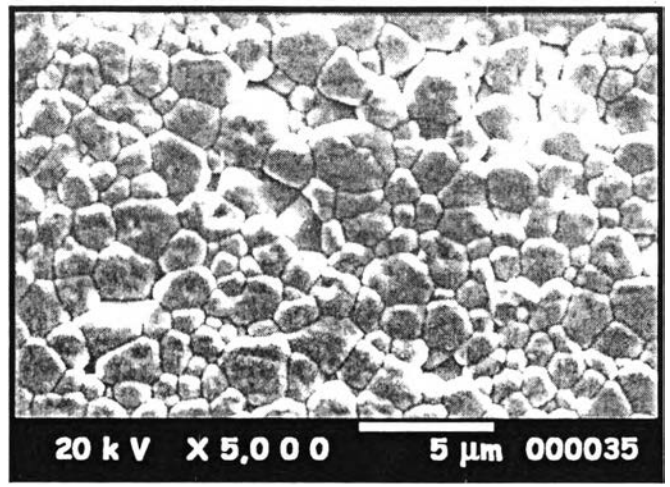

Fig. 4.5 j. SEM micrograph of 0.5 at% K_2O doped PLZT (3/52/48)

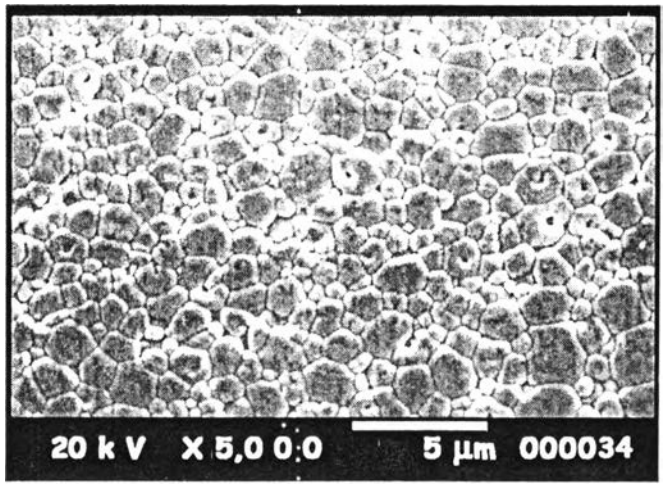

Fig. 4.5 k. SEM micrograph of 0.5 at% Li_2O doped PLZT (3/52/48) ceramics

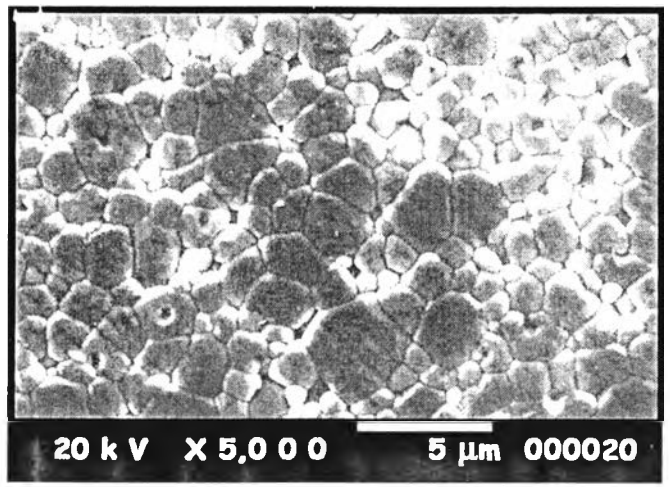

Fig. 4.5 l. SEM micrograph of 0.5 at% Mn_2O_3 doped PLZT (3/52/48) ceramics

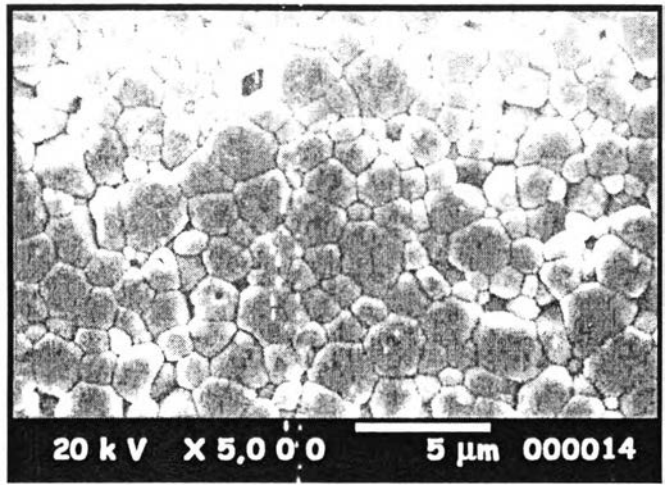

Fig. 4.5 m. SEM micrograph of 0.5 at% Nb_2O_5 doped PLZT (3/52/48) ceramics

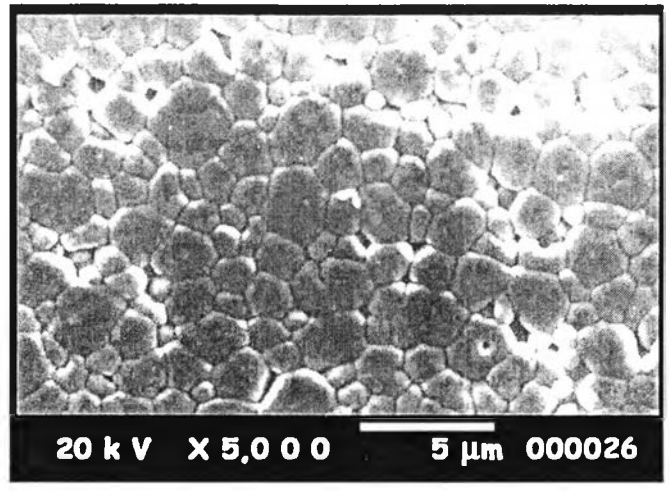

Fig. 4.5 n. SEM micrograph of 0.5 at% NiO doped PLZT (3/52/48) ceramics

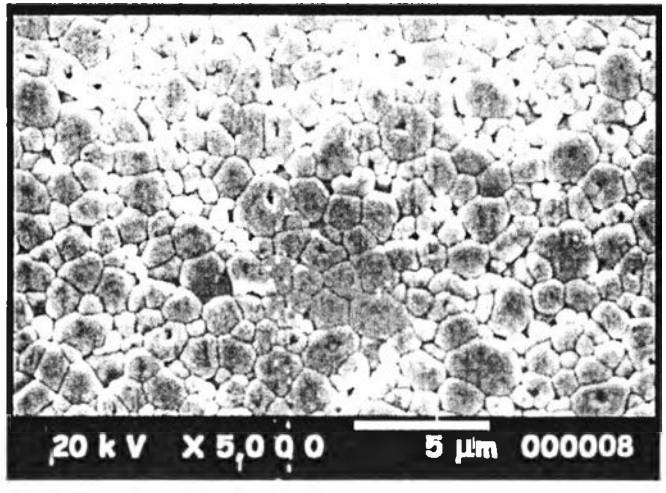

Fig. 4.5 o. SEM micrograph of 0.5 at% SeO_2 doped PLZT (3/52/48) ceramics

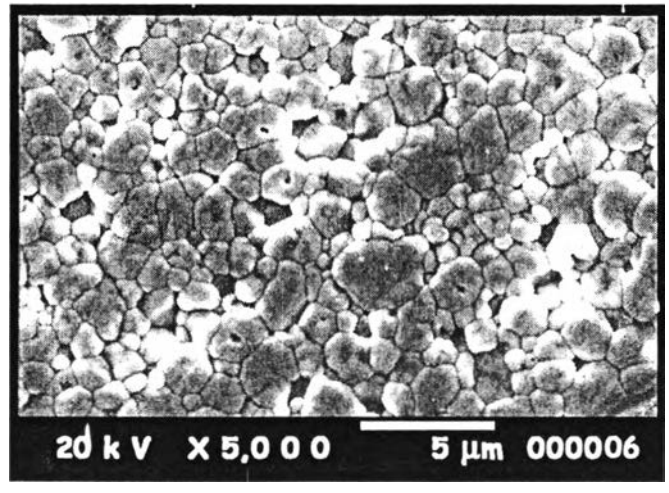

Fig. 4.5 p. SEM micrograph of 0.5 at% SnO_2 doped PLZT (3/52/48) ceramics

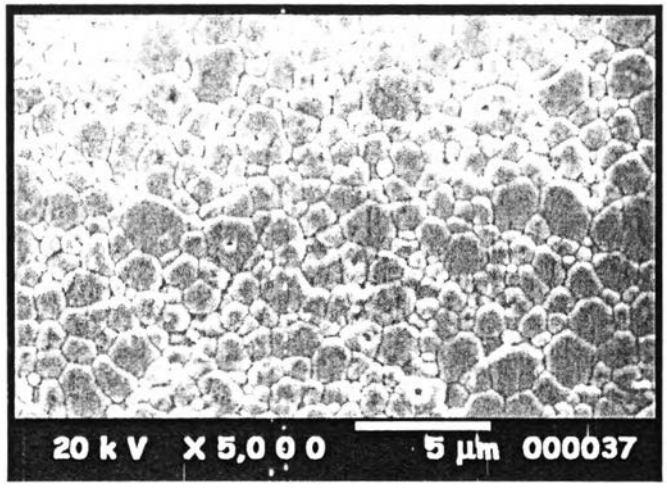

Fig. 4.5 q. SEM micrograph of 0.5 at% SrO doped PLZT (3/52/48) ceramics

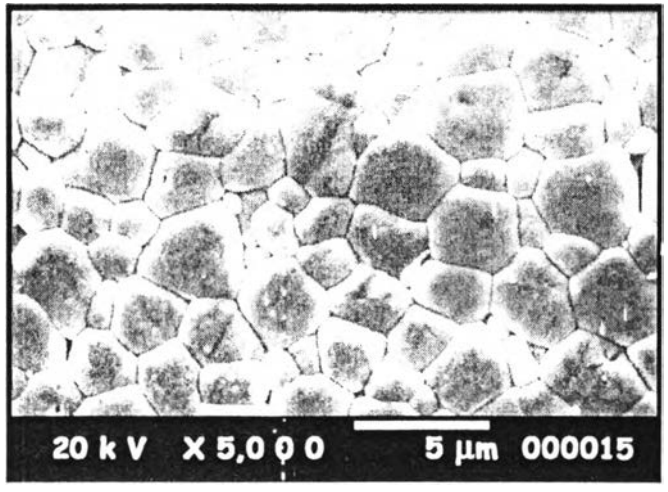

Fig. 4.5 s. SEM micrograph of 0.5 at% WO_3 doped PLZT (3/52/48) ceramics

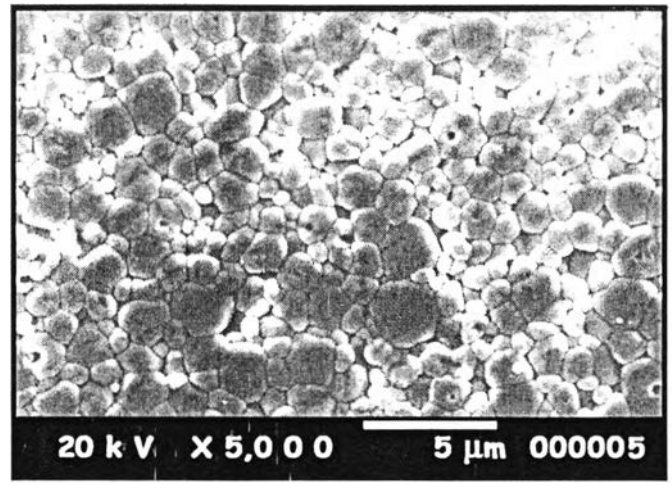

Fig. 4.5 r. SEM micrograph of 0.5 at% V_2O_5 doped PLZT (3/52/48) ceramics

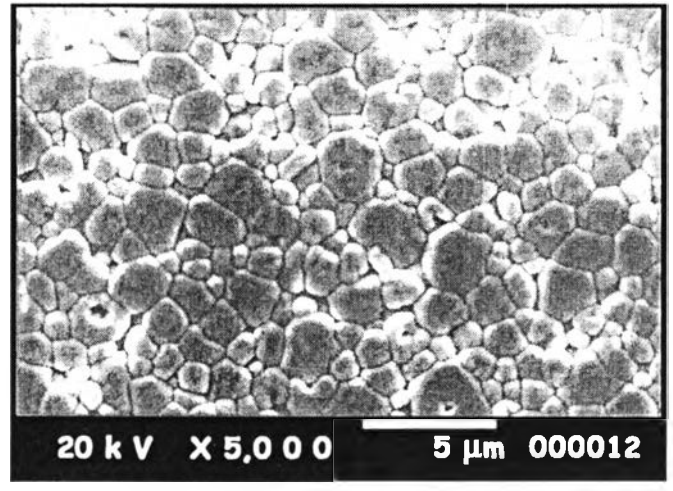

Fig. 4.5 t. SEM micrograph of 0.5 at% Y_2O_3 doped PLZT (3/52/48) ceramics

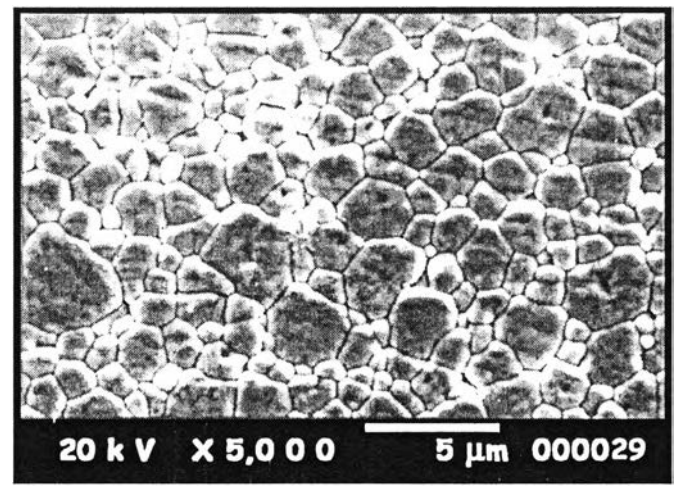

Fig. 4.5 u. SEM micrograph of 0.5 at% ZnO doped PLZT (3/52/48) ceramics

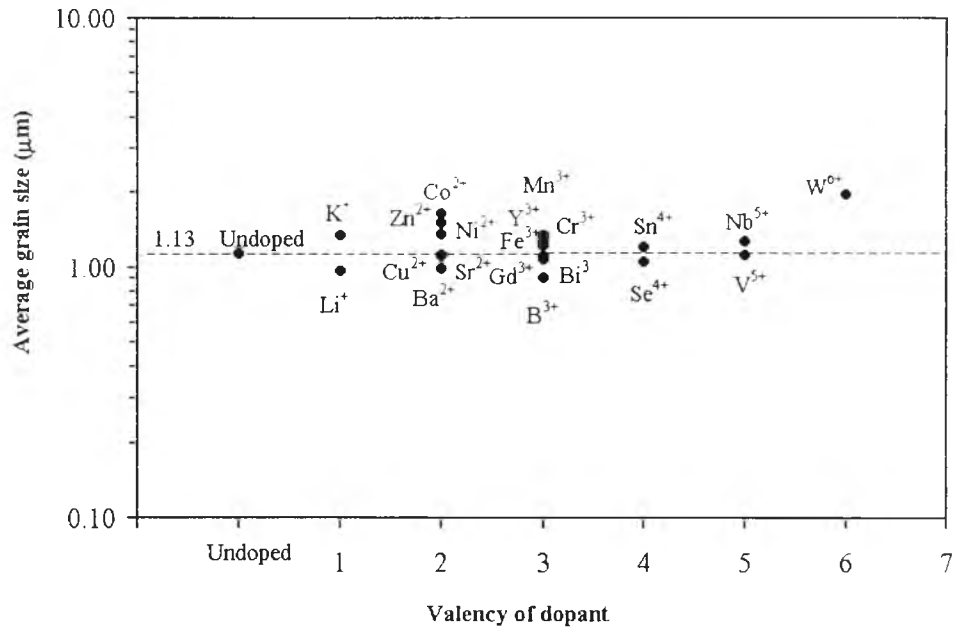

Fig. 4.6 Dopant valency as a function of the average grain size of 0.5 at% doped PLZT (3/52/48) ceramics

Fig. 4.6 shows dopant valency as a function of the average grain size of 0.5 at% doped PLZT (3/52/48) ceramics. With the exception of WO_3, it seems that the rest of the dopants employed have no significant effect on the average grain size. However, the anomalous grain growth observed in the 0.5 at% WO_3 doped PLZT (3/25/48) ceramic which needs further confirmation.

4.5 Doping effect on dielectric constant

Room temperature dielectric constant (K) and the dissipation factor (D) of poled samples measured at five different frequencies, 100 Hz, 1 kHz, 10 kHz, 100 kHz and 1 MHz, are shown in Table 4.4

Table 4.4 Dielectric constant (K) and dissipation factor (D) of undoped and 0.5 at% doped PLZT (3/52/48) ceramics

Doping	100 Hz		1 kHz		10 kHz		100 kHz		1 MHz	
Ions	K	D	K	D	K	D	K	D	K	D
Mn^{3+}	1308	0.0063	1295	0.0064	1311	0.0067	1299	0.0077	1314	0.0128
Cr^{3+}	1448	0.0187	1434	0.0191	1395	0.0202	1374	0.0212	1426	0.0291
V^{5+}	1471	0.0205	1456	0.0209	1411	0.0224	1365	0.0273	1338	0.0995
Ni^{2+}	1476	0.0202	1461	0.0206	1416	0.0217	1372	0.0237	1355	0.0324
Y^{3+}	1478	0.0215	1463	0.0219	1477	0.0228	1428	0.0271	1425	0.0438
Co^{2+}	1480	0.0150	1466	0.0153	1432	0.0165	1398	0.0185	1391	0.0271
W^{6+}	1489	0.0242	1475	0.0247	1422	0.0253	1370	0.0269	1350	0.0341
K^{+}	1506	0.0199	1491	0.0203	1445	0.0214	1400	0.0231	1385	0.0284
Cu^{2+}	1513	0.0190	1498	0.0194	1456	0.0204	1412	0.0223	1400	0.0291
Bi^{3+}	1524	0.0212	1509	0.0216	1460	0.0230	1411	0.0251	1393	0.0349
Fe^{3+}	1530	0.0204	1515	0.0208	1494	0.0217	1422	0.0236	1404	0.0308
Sn^{4+}	1540	0.0198	1525	0.0202	1478	0.0217	1430	0.0236	1412	0.0285
Nb^{5+}	1547	0.0247	1532	0.0252	1474	0.0281	1417	0.0772	1227	0.3667
Undoped	1552	0.0204	1537	0.0208	1489	0.0221	1435	0.0244	1433	0.0367
Li^{+}	1566	0.0202	1551	0.0206	1506	0.0217	1458	0.0231	1441	0.0282
Se^{4+}	1585	0.0197	1570	0.0201	1522	0.0218	1473	0.0237	1455	0.0294
B^{3+}	1610	0.0205	1594	0.0209	1544	0.0223	1493	0.0242	1482	0.0298
Zn^{2+}	1619	0.0203	1603	0.0207	1556	0.0217	1507	0.0232	1491	0.0295
Ba^{2+}	1626	0.0214	1610	0.0218	1562	0.0231	1508	0.0250	1489	0.0319
Sr^{2+}	1645	0.0207	1629	0.0211	1561	0.0224	1525	0.0226	1508	0.0301
Gd^{3+}	1647	0.0189	1631	0.0193	1582	0.0209	1533	0.0232	1517	0.0301

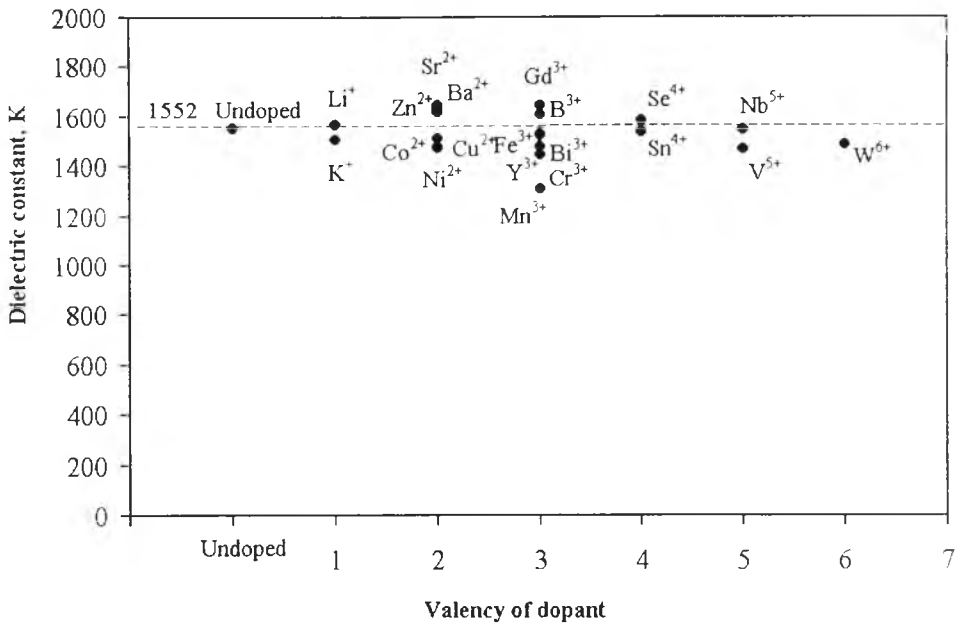

Fig. 4.7 Dielectric constant as a function of dopant valency of 0.5 at% doped PLZT (3/52/48) ceramics

Dielectric constant measured at a frequency of 100 Hz shows the maximum value at 1647 for Gd^{3+} doped PLZT ceramic and the minimum at 1308 for Mn^{3+} doped PLZT ceramic. Fig. 4.7 shows the variation of dielectric constants with the valencies of dopant. It can be seen that there is no significant change in dielectric constant of PLZT ceramics with dopants, except for Mn^{3+} of which the low dielectric constant is observed. This result is partially due to the lower relative density.

4.6 Doping effect on piezoelectric constant

The piezoelectric constant (d_{33}) of all the samples were measured with a d_{33} meter (Berlincourt Piezo d-meter Model CADT) at an applied vibration frequency of 120 Hz. The piezoelectric constants of undoped and doped PLZT ceramics are shown in Table 4.5.

Table 4.5 Piezoelectric constants (d_{33}) of undoped and 0.5 at% doped PLZT (3/52/48) ceramics

Doping Ions	d_{33} (x 10^{-12} m/V)
Mn^{3+}	168
V^{5+}	273
Co^{2+}	312
Cr^{3+}	314
Undoped	315
K^{+}	323
Bi^{3+}	332
B^{3+}	333
Fe^{3+}	341
Cu^{2+}	343
Se^{4+}	343

Doping Ions	d_{33} (x 10^{-12} m/V)
Ni^{2+}	347
Sr^{2+}	350
Sn^{4+}	353
Gd^{3+}	357
Y^{3+}	357
Li^{+}	358
Nb^{5+}	372
Zn^{2+}	382
W^{6+}	384
Ba^{2+}	395

Fig. 4.8 shows the variation of piezoelectric constants with dopant valencies. It can be seen that the piezoelectric constants show no significant difference in all the samples excepted that of Mn dopant. This indicates that type of the doping ions and the level of concentration (0.5 at%) employed do not significantly affect the piezoelectric property of the PLZT ceramics. This result is similar to the previous investigation by Tanimura in 1988.[2] The freak effect of Mn doped PLZT ceramics on piezoelectric constant needs to be further studied for confirmation.

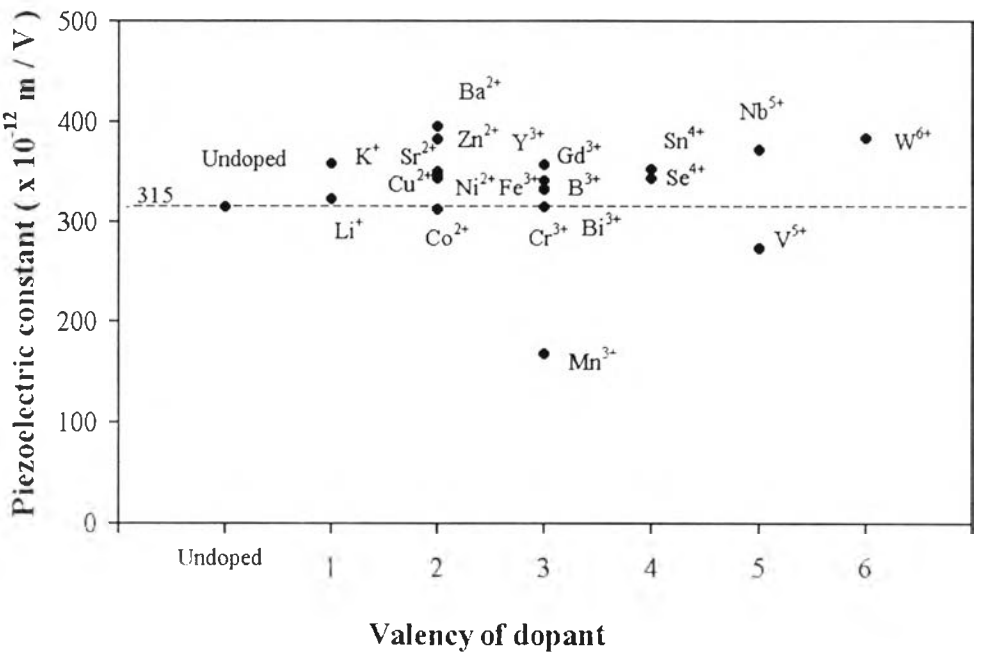

Fig. 4.8 Piezoelectric constant as a function of dopant valency of 0.5 at% doped PLZT (3/52/48) ceramics

4.7 Doping effect on photovoltaic properties

Photovoltaic properties of poled PLZT samples were measured under the illumination of high intensity UV light. Light intensity using in this study was 2.10 mW/cm^2. Photovoltage and photocurrent were determined from the plot between the measured current with the applied voltage from -100 to +100 V, while the samples were being illuminated is shown in Fig. 4.9. Photovoltage (E_{ph}) and photocurrent (I_{ph}) were estimated from an intercept of voltage and current axes, respectively. Photoconductance (G_{ph}) was determined from the slope of I_{ph}-E_{ph} curve of each doped PLZT cermaics, which was in the order of 10^{-12} ohm^{-1} Table 4.6 shows the variation of photovoltaic properties with dopants.

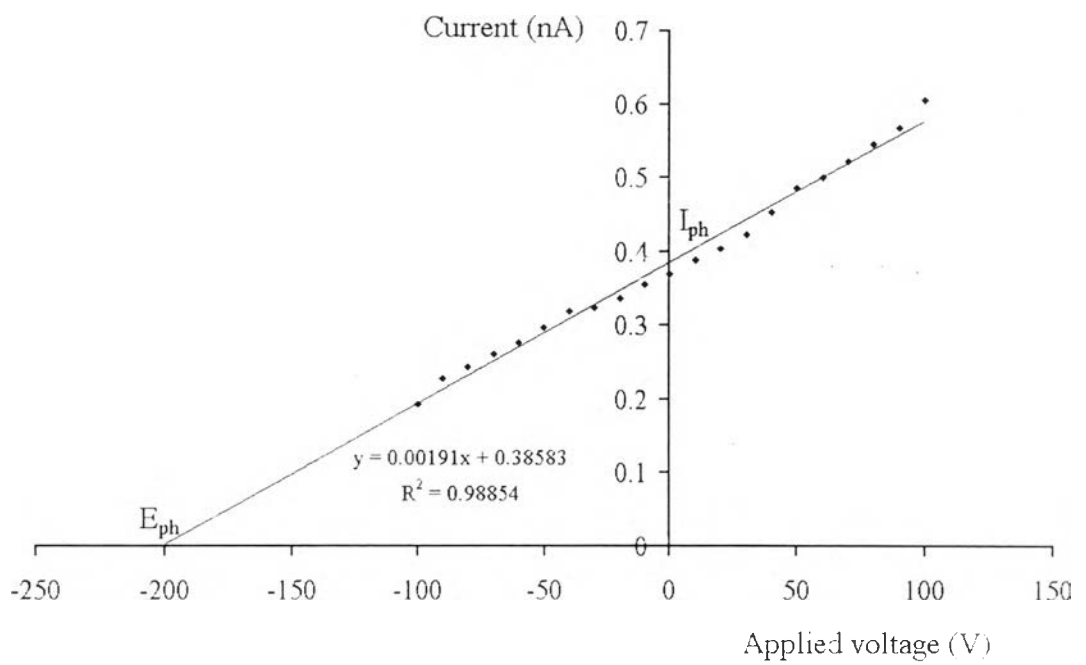

Fig. 4.9 Plotting curve of photocurrent as a function of an applied voltage

Table 4.6 Photovoltage (E_{ph}), photocurrent (I_{ph}), photoconductance (G_{ph}) and photovoltaic power (P_{ph}) of undoped and 0.5 at% doped PLZT (3/52/48) ceramics

Doping Ions	E_{ph} (V/cm)	I_{ph} (nA/cm)	G_{ph} x 10^{-12} (ohm^{-1})	P_{ph} x 10^{-9} (VA/cm^2)
Co^{2+}	46	0.02	0.76	0.92
Ni^{2+}	53	0.02	0.60	1.06
Cr^{3+}	73	0.03	0.64	2.19
Mn^{3+}	323	0.17	0.90	54.91
Zn^{2+}	346	0.39	1.96	134.94
Cu^{2+}	372	0.13	0.62	48.36
Li^{+}	424	0.34	1.47	144.16
B^{3+}	470	0.50	1.87	235.00
Fe^{3+}	476	0.11	0.39	52.36
V^{5+}	498	0.21	0.73	104.58
Undoped	590	0.60	1.90	354.00
Y^{3+}	593	0.42	1.23	249.06
Se^{4+}	659	0.40	1.04	263.60
K^{+}	667	0.42	1.10	280.14
Nb^{5+}	707	0.64	1.59	452.48
Sn^{4+}	740	0.43	1.09	318.20
W^{6+}	761	0.51	1.21	388.11
Bi^{3+}	786	0.42	0.99	330.12
Sr^{2+}	787	0.41	0.92	322.67
Ba^{2+}	845	0.59	1.28	498.55
Gd^{3+}	845	0.55	1.14	464.75

Fig. 4.10 shows the relation between the photovoltage and the photocurrent of PLZT ceramics. A dashed line in Fig. 4.10 represents the constant power curve (photovoltaic power = E_{ph} x I_{ph}) corresponding to the undoped PLZT. Dopants divided into five groups as discussed in page 13, give different effects of photovolaic properties. It is clearly seen that donor A- and B-sites as well as isovalence dopants provide higher photovoltaic properties while 3d transition dopants decrease the properties as compared to the undoped PLZT. The acceptor dopants provide photovoltaic properties in between the 3d transition and donor groups.

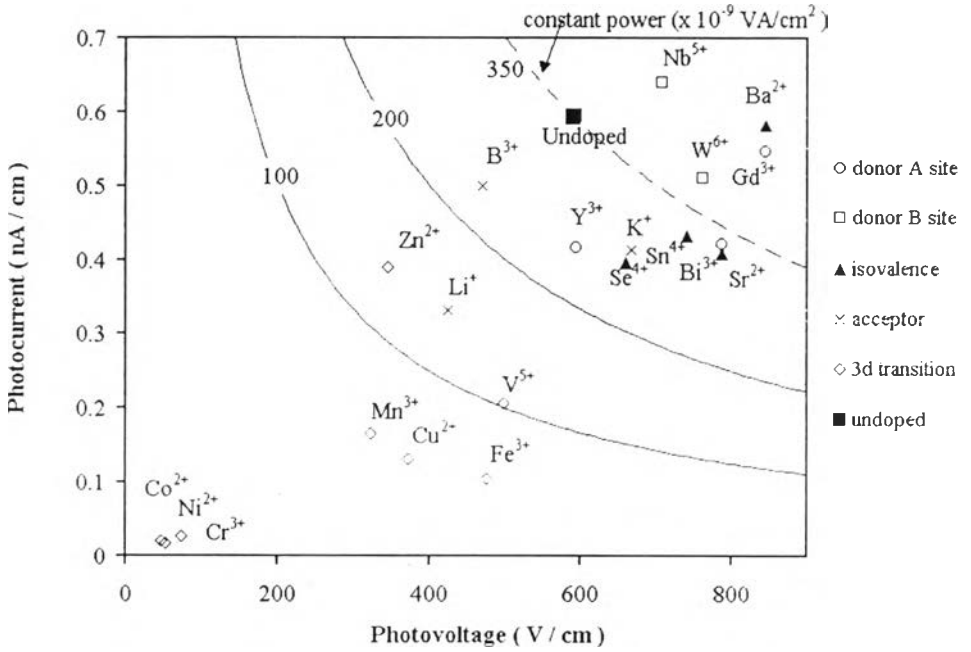

Fig. 4.10 Photovoltaic response as a function of doping ions

4.8 Doping effect on photostrictive properties

Photostrictive properties of all the samples are shown in Table 4.7. It must be noted that photo-induced strain or photostrictive strain were calculated using the following equation:[2,3]

$$x_{ph} = d_{33} \times E_{ph} \quad (1.1)$$

where x_{ph} is photo-induced strain
d_{33} is piezoelectric constant
E_{ph} is photovoltage

Table 4.7 Photo-induced strain calculated from $d_{33} \times E_{ph}$ for 0.5 at% doped PLZT (3/52/48) ceramics

Doping Ions	d_{33} $x10^{-12}$ (m/V)	E_{ph} (V/cm)	X_{ph} ($x\ 10^{-5}$)
Co^{2+}	312	46	0.14
Ni^{2+}	347	53	0.18
Cr^{3+}	314	73	0.23
Mn^{3+}	168	323	0.54
Cu^{2+}	343	372	1.28
Zn^{2+}	382	346	1.32
V^{5+}	273	498	1.36
Li^{+}	358	424	1.52
B^{3+}	333	470	1.57
Fe^{3+}	341	476	1.62
Undoped	315	590	1.86
Y^{3+}	357	593	2.12
K^{+}	323	667	2.15
Se^{4+}	343	659	2.26
Bi^{3+}	332	786	2.61
Sn^{4+}	353	740	2.61
Nb^{5+}	372	707	2.63
Sr^{2+}	350	787	2.75
W^{6+}	384	761	2.92
Gd^{3}	357	845	3.02
Ba^{2+}	395	845	3.34

Piezoelectric constant and photo-induced strain are found to be proportional to photovoltage in PLZT ceramics incorporating dopants as shown in Fig. 4.11 and 4.12. Donor A-and B-sites as well as isovalence dopants (Ba^{2+}) are found to increase photostriction in PLZT ceramic. A decrease in photostrictive property is found in PLZT doped with 3d transition elements. Doping with acceptor ions provides photo-induced strain in between. This finding is similar to the previous investigations by Tanimura in 1988.[2]

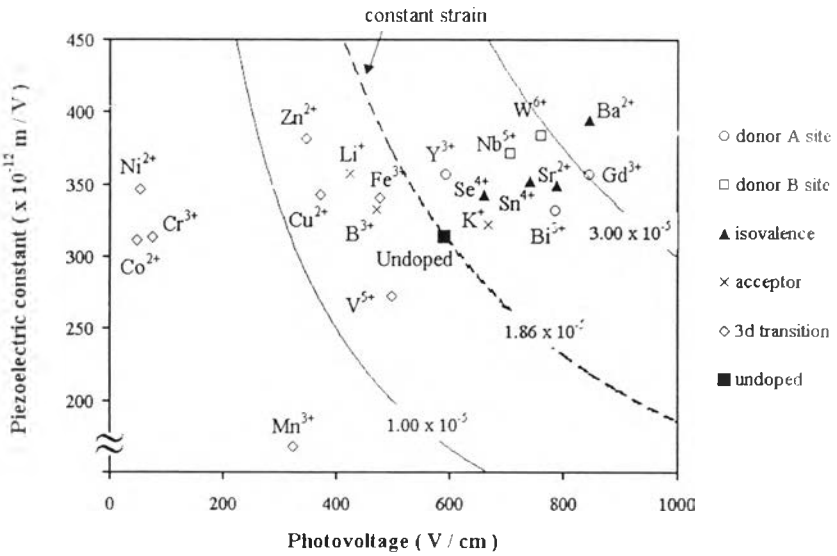

Fig. 4.11 Variation of photovoltage with piezoelectric constant

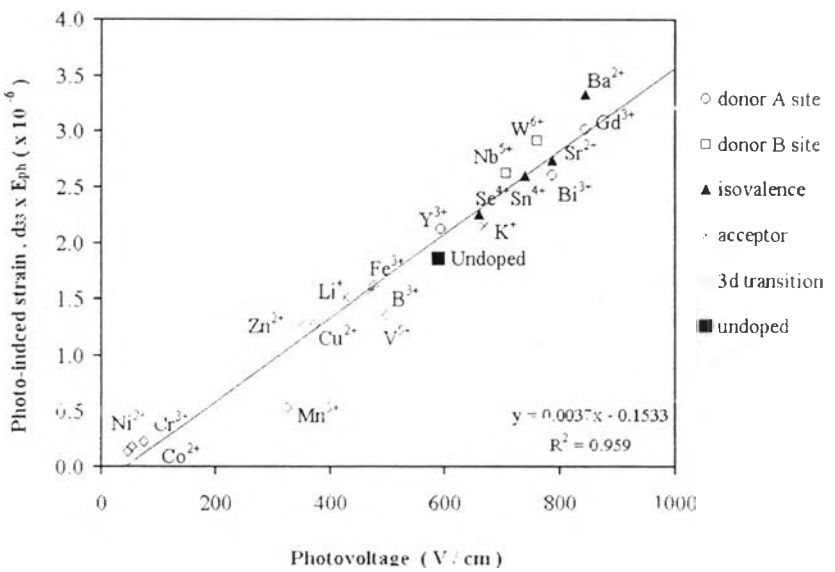

Fig. 4.12 Photo-induced strain as a function of photovoltage in PLZT (3/52/48) ceramics

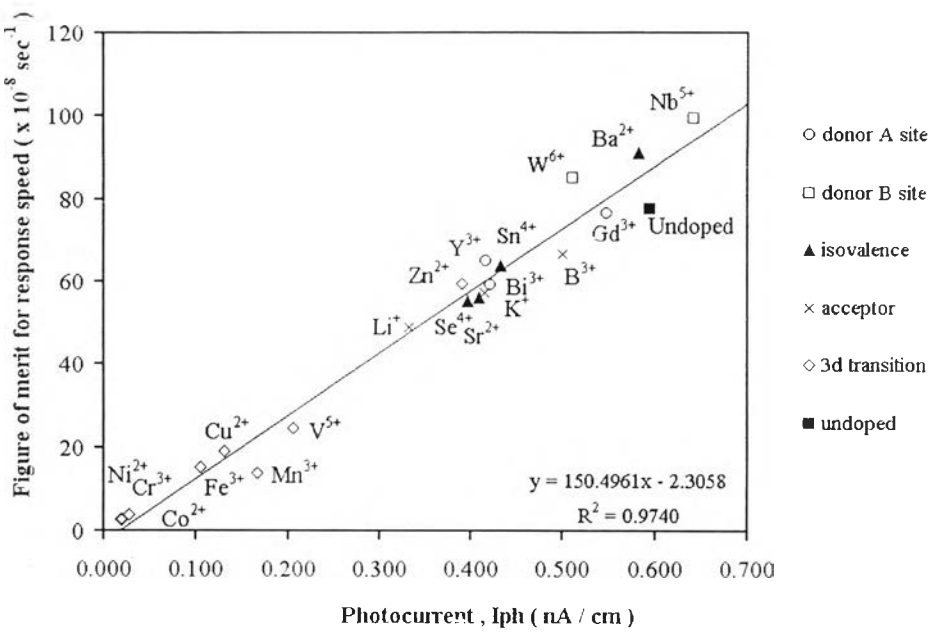

Fig. 4.13 Response speed, d_{33} x I_{ph} / C , as a function of photocurrent in undoped and 0.5 at% doped PLZT (3/52/48) ceramics

The figure of merit for response speed calculated by d_{33} I_{ph} / C is shown in Fig. 4.13. It was found that photocurrent is proportional to the merit of response speed. The maximum value was found in Nb^{5+} doped PLZT.

The effect of doping on PLZT (3/52/48) ceramics can be summarized as follows:

1. Donor A-and B-sites were found to increase photovoltage, photocurrent, and photo-induced strain as compared to undoped PLZT ceramics. These dopants are suitable for the applications which required fast response speed.
2. Isovalence dopant especially Ba^{2-} provides the same effect as donor A- and B- sites.
3. Doping with acceptor ions results in lower photovoltaic and photostrictive properties.
4. Decreasing and scattering results in photovoltaic and photostrictive properties are found in PLZT ceramics doped with 3d transition elements.

4.9 Doping effect on optical absorption edge

Optical transmission spectra of undoped PLZT (3/52/48) sample measured at room temperature with an excitation wavelength of 200-900 nm by a UV/Vis spectrophotometer is shown in Fig. 4.14. Determination of the optical absorption edge or energy band gap has been described in chapter 2. The tangential line at high α region of the $h\nu$ *vs* $(\alpha\ h\ \nu)^{1/2}$ curve is extrapolated to intercept the h ν axis as shown in Fig. 4.15. This intercept value is defined as the energy band gap.

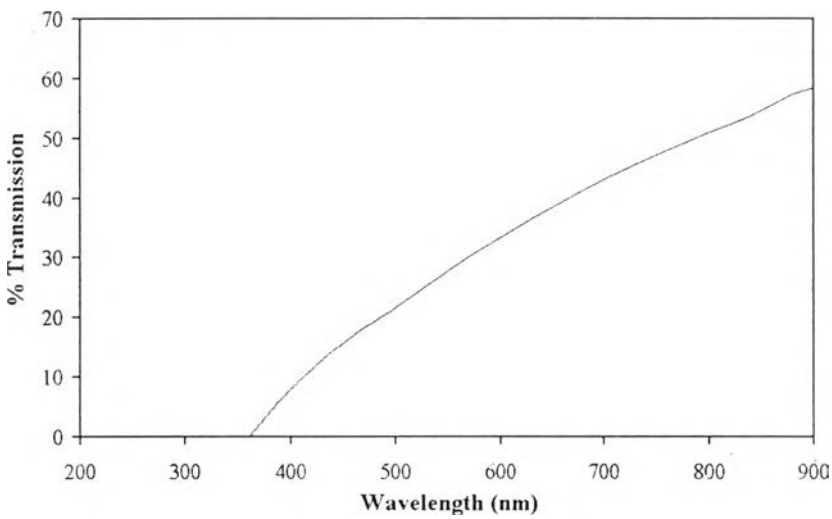

Fig. 4.14 Optical transmission spectra of PLZT (3/52/48) ceramics thin section

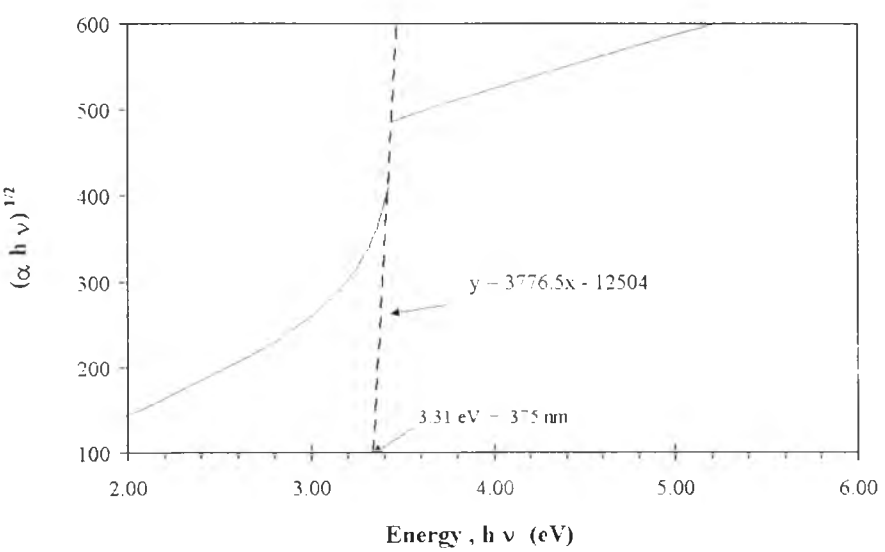

Fig. 4.15 Square roots of (α h ν) as a function of (hν) of PLZT (3/52/48) ceramics thin section

Optical absorption edge of all PLZT samples was measured and calculated using the method described above and was shown in Table 4.8.

Table 4.8 Optical absorption edge of undoped and doped PLZT (3/52/48) ceramics

Doping Ions	absorption edge (nm)
Bi^{3+}	370
Co^{2+}	370
Li^{+}	370
Ni^{2+}	370
Sr^{2+}	370
undoped	375
B^{3+}	375
Cr^{3+}	375
K^{+}	375
Mn^{3+}	375
Se^{4+}	375

Doping Ions	absorption edge (nm)
Sn^{4+}	375
Y^{3+}	375
Zn^{2+}	375
Ba^{2+}	380
Fe^{3+}	380
V^{5+}	380
Gd^{3+}	385
Nb^{5+}	385
Cu^{2+}	390
W^{6+}	390

The relationship between valency of dopant and the optical absorption edge is shown in Fig. 4.16. The maximum value of absorption edge is found at 390 nm for Cu^{2+} and W^{6+} doped PLZT ceramics. The next interesting dopants are Gd^{3+} and Nb^{5+} which exhibit the absorption edge value of 385 nm, higher than the undoped. The remainders insignificantly shift the absorption edge of PLZT ceramic.

In spite of the difference in the type of doping ions, the value of the absorption edge of Cu^{2+} doped PLZT is same as W^{6+}. The previous investigation upon the effect of Cu^{2+} doping on the optical properties of PLZT (8/65/35) was reported by Bryknar, Z. in 1998.[55] The transmission spectra in his work showed the absorption edge shifted to the visible region when PLZT ceramic was doped with 1 wt% of CuO. The shift in absorption edge may be caused by the reduction of CuO to Cu_2O. The band gap energy of Cu_2O is 2.1 eV[40], hence lower than 3.3 eV of PLZT ceramics.

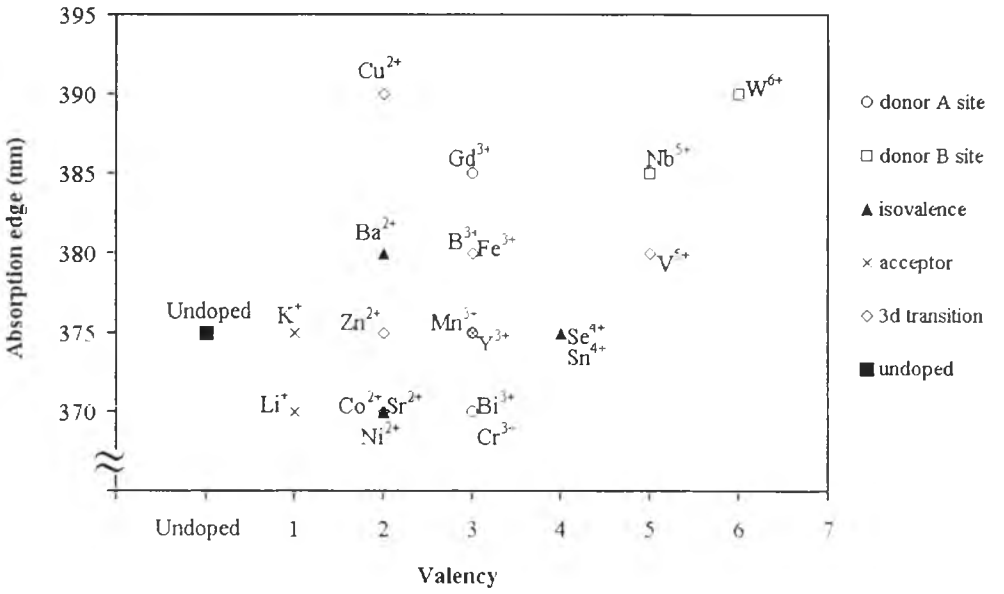

Fig. 4.16 Scatter diagram of absorption edge as a function of dopant valency in PLZT (3/52/48) ceramics